

# Reliable experimental certification of one-way Einstein-Podolsky-Rosen steering

Qiang Zeng,<sup>1,2</sup> Jiangwei Shang,<sup>1,\*</sup> H. Chau Nguyen,<sup>3,†</sup> and Xiangdong Zhang<sup>1,‡</sup>

<sup>1</sup>Key Laboratory of Advanced Optoelectronic Quantum Architecture and Measurement of Ministry of Education, School of Physics, Beijing Institute of Technology, Beijing 100081, China

<sup>2</sup>Centre for Quantum Computation and Communication Technology (Australian Research Council), Centre for Quantum Dynamics, Griffith University, Brisbane, Queensland 4111, Australia

<sup>3</sup>Naturwissenschaftlich-Technische Fakultät, Universität Siegen, 57068 Siegen, Germany

(Dated: October 27, 2020)

Quantum steering is a recently-defined form of quantum correlation which lays at the heart of quantum mechanics. In difference from other types of quantum correlations, quantum steering is inherently asymmetric, which presents in one direction but may not in the other direction in a bipartite system. Recently, a conclusive experimental demonstration of this directional nature of quantum steering has been carried out, yet requires a crucial use of a qutrit party to overcome the ambiguous assumptions existing in previous experiments. Therefore, a reliable experimental certification of one-way steering in genuine qubit systems still remains an challenging question. Here, we report such an experiment demonstrating one-way steering for the two-qubit entangled system based on a newly-developed orbital angular momentum platform. Our scheme and results thus resolve the subtlety in the dimensionality and further the existing data of previous demonstrations, and provide a universal method to characterize one-way steering effect for two-qubit states.

*Introduction.*—Back in 1935, Einstein, Podolsky, and Rosen (EPR) [1] proposed a Gedanken experiment to demonstrate that quantum mechanics allows for the so-called “spooky action at a distance.” To capture the idea of EPR’s work, Schrödinger later coined the word *steering*. Naively, steering indicates that the choice of measurements on one side of a bipartite system can specify the possible conditional states of the other. It remained as an informal intuition until Wiseman *et al.* proposed the rigorous and operational definition for steering from the perspective of quantum information theory [2–4].

As of nowadays, quantum steering [5–16] is the last member in the family of three types of quantum correlations; the other two are entanglement [17, 18] and Bell nonlocality [19–21]. Among these three nonlocalities, steering is rather special in that its definition possesses inherent asymmetry [22–29]. Namely, in an entangled system, it is possible that one subsystem is able to steer the other yet the reverse is not possible. In the language of theoretical information tasks, the steerability of one party to the other is defined as the ability to remotely generate ensembles that could not be explained by means of postprocessing on local hidden states (LHS) at the other party. While, the one-way steerability (1WS) means that the role of the two parties cannot be exchanged. This directional nature is sometimes a natural advantage in certain quantum information protocols [16].

Demonstration of this curious asymmetry of steerability is in fact challenging. This is because one-way steerable states form a rather thin layer of states between unsteerable states and two-way steerable states [30], demanding for rather subtle parameter-manipulation in experiments. Though there were early experiments demonstrating one-way steering [31–33], a conclusive experiment was carried out very recently [34]. This latest ex-

periment takes advantage of a qubit-qutrit system, with the extra dimensionality embedding in order to get more flexibilities. Paradoxically, one-way steering certification in a two-qubit system turns out to be more difficult than that in higher-dimensional systems since the asymmetric form of state is often attained by introducing an extra dimension as ancillas. Even though the extra dimension on one party is employed in a trivial way, i.e., as the vacuum-subspace rather than photon-subspace, still the need of the third dimension was crucial. On the other hand, experiments that demonstrate one-way steerability for two-qubit systems with ideal measurements have committed additional assumptions on the states. More precisely, it is often assumed that the prepared states depend on few parameters and measurement space [4, 35, 36]; see also the discussions in Ref. [34]. Our analysis, however, shows that these assumptions turn out to be stronger than expected and are commonly violated in the experimental demonstration, resulting in the ambiguities showing in the existing data; see detailed analysis in S1 of Supplemental Material [37]. These all question the ability to reliably generate and characterize one-way steerable states if the dimension of the system is limited to two.

In this work, we address the one-way steering experiment in a genuine qubit-qubit system based on an orbital angular momentum (OAM) platform. OAM system [38–43] is widely applicable in quantum information studies, and proved to be advantageous in introducing tunable noise [44]. We achieve a new family of states and characterize the one-way steerability, taking advantage of a recent advance in the theoretical understanding of quantum steering in qubit systems [30]. By preparing the one-way steerable states in a genuine two-qubit system, we thus resolve the ambiguities in the old data with ideal measurements as well as the subtlety in the ancil-

lary dimension, so that establish a reliable experimental certification of one-way steering for two qubits. It is also worthy noting that both our experimental setup and theoretical analysis are adaptive to general two-qubit states, so the method we are presenting in this work provides a universal way to characterize one-way steering effect for two-qubit states.

*The targeted states.*—Consider a bipartite state  $\rho$  shared by two parties  $A$  and  $B$ . In this work, we consider a family of states which is simply the mixture of the singlet state with a product state, i.e.,

$$\rho = p|\Psi^+\rangle\langle\Psi^+| + (1-p)\rho_r \otimes \frac{\mathbb{I}}{2}, \quad (1)$$

where  $|\Psi^+\rangle = (|0,1\rangle + |1,0\rangle)/\sqrt{2}$ , and  $\rho_r = \frac{1}{2}(\mathbb{I} + r\sigma_z)$  with  $\sigma_z$  being the Pauli operator. The free parameters  $p$  and  $r$  can take values from 0 to 1.

To quantify the steerability from  $A$  to  $B$  of the state, one defines

$$r_{AB}(\rho) = \max_x \{x \geq 0 : \rho^{(x)} \text{ is unsteerable}\}, \quad (2)$$

where  $\rho^{(x)} = x\rho + (1-x)(\mathbb{I}_A \otimes \rho_B)/2$  and  $\rho_B = \text{tr}_A(\rho)$  is the reduced state for party  $B$ . One defines  $r_{BA}(\rho)$  in the similar way. It is clear that  $r_{AB}$  and  $r_{BA}$  fully characterize the steering of  $\rho$ :  $\rho$  is steerable from  $A$  to  $B$  (or from  $B$  to  $A$ ) if and only if  $r_{AB}(\rho) < 1$  ( $r_{BA}(\rho) < 1$ , respectively.) Clearly, it is not obvious that  $r_{AB}(\rho)$  can be computed from its definition. However, in Ref. [30], the quantity  $r_{AB}(\rho)$  is given a geometrical meaning, implied in its name as critical radius of steering, and an algorithm to compute its value for an arbitrary state is also given. In fact, states in the form of Eq. (1) carry an axial symmetry [30], which allows for an easy characterization of the one-way steerable areas as illustrated in Fig. 1. As we mentioned early, the 1WS area (red) is relatively small as compared to other regions, thus precise parameter manipulation and effective noise control are required in the experimental demonstration.

*Experimental setup.*—A sketch of the experiment platform is shown in Fig. 2, and the real scale version is provided in S2 of Supplemental Material [37]. In order to obtain the maximally entangled OAM state  $|\Psi^+\rangle$ , we utilize a pulsed laser with pulse length of 1 fs to impact a type-I BBO crystal. The pulsed laser centers at 400 nm with the power of 180 mw. A half-wave plate (HWP) is inserted to align the photons at horizontal polarization for fulfilling the requirement of the spatial light modulator (SLM). The subsequent lens with 300 mm focal length are to project the entangled photons onto SLM 1, where an animation is loaded. A proper modulating process requires the image size of the incident photons and the scale of the SLM match, so we set the distance between the lens and SLM 1 as 350 mm, by which we render the image of the incident photons on the subsequent SLM 1 with the photons being properly shrunk. Likewise, the

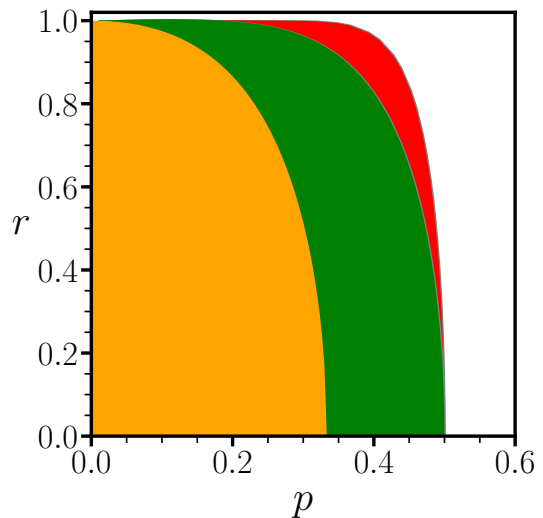


FIG. 1. Steering areas for the two-parameter axial states as defined in Eq. (1). The orange region represents the separable states, and the two-way unsteerable states lie in the green region. The 1WS region is indicated in red color, which is relatively small as compared to other regions.

following lens and SLM 2 keep the same structure. However, instead of using animation, we set static holograms on SLM 2, which is to accomplish the task of state tomography upon combining with the single-mode fiber. Besides, in order to attain a high efficiency of the collecting photons, we insert a pair of lenses with 250 mm focal length in front of the two collectors, where two micro lenses with 7.5 mm focal length are also embedded respectively (not shown in the sketch).

Next, we explain how to construct the corresponding animations giving the specified parameters  $p$  and  $r$ . In our scheme, the qubit is encoded with the OAM modes  $l = \pm 2$ , namely,  $|0\rangle \equiv |l = -2\rangle$  and  $|1\rangle \equiv |l = 2\rangle$ . Then, an over-complete tomography scheme [45] with six measurement outcomes on each side is implemented to characterize the input axial states. Specifically, the six measurement outcomes are written as  $|X_m\rangle = |0\rangle + (-1)^m|1\rangle$ ,  $|Y_n\rangle = |0\rangle + i(-1)^n|1\rangle$ ,  $|Z_0\rangle = |0\rangle$ , and  $|Z_1\rangle = |1\rangle$ , with  $m, n \in \{0, 1\}$ . Based on these expressions, the maximally mixed state can be decomposed as [46]

$$\frac{\mathbb{I}}{2} = \frac{1}{6} \left( \sum_{m=0}^1 |X_m\rangle\langle X_m| + \sum_{n=0}^1 |Y_n\rangle\langle Y_n| + \sum_{l=0}^1 |Z_l\rangle\langle Z_l| \right). \quad (3)$$

In addition, the 1WS factor in the axial state can be expressed as

$$\rho_r \otimes \frac{\mathbb{I}}{2} = \left[ r|0\rangle\langle 0| + (1-r)\frac{\mathbb{I}}{2} \right] \otimes \frac{\mathbb{I}}{2}. \quad (4)$$

Obviously, 36 holograms are needed to be in the random pool, which corresponds to the isotropic noise. We denote the sample probability of this isotropic part as

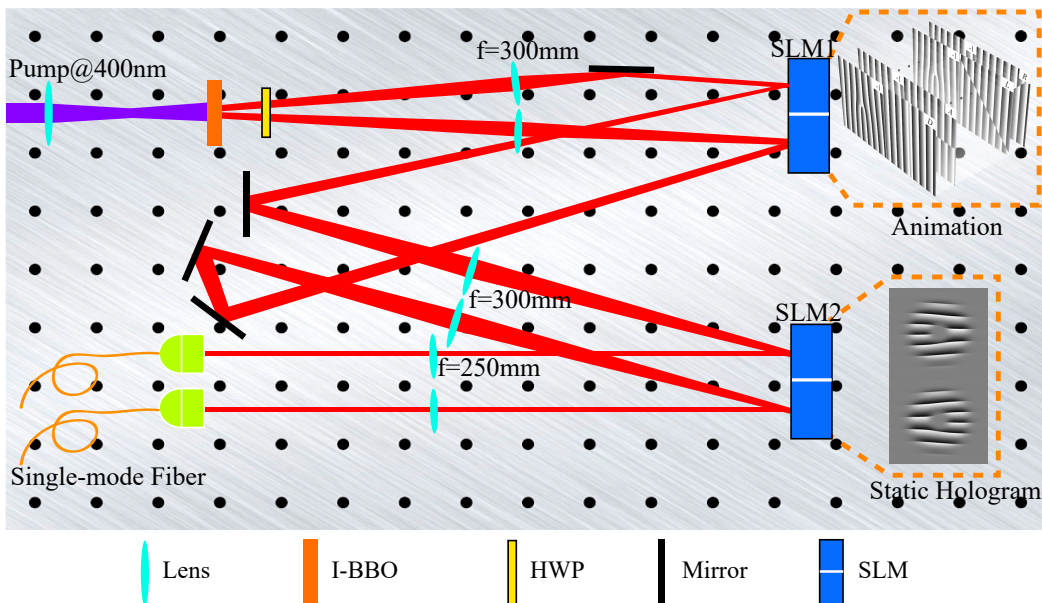


FIG. 2. Sketch of the experimental platform. A standard type-I spontaneous parametric down-conversion (SPDC) with the efficiency of around 15% is employed to generate the OAM entanglement. In order to obtain as many as photon pairs without losing high-order modes, a medium thickness (3 mm) of a non-linear type-I BBO crystal is adopted. As for the animation configuration, in each path, the size of the hologram is  $960 \times 180$  (pixel) with the exposure time being 0.02 s. We set the number of sampling as  $N = 800$  to guarantee that every hologram being fully sampled even if  $p$  and  $r$  are small. Then, the coincidence measurement accumulation time is set to be 20 s to ensure that the animation is fully applied. Since each of the two SLMs has a loss of 49.6% and the collecting efficiency is 70.1%, the overall efficiency of the experiment setup is 17.2%. Pumper: coherent Chameleon (centered at 800 nm). HWP: half-wave plate. SLM: spatial light modulator. Collector: photon to fiber collector embedded with narrow bandwidth filter ( $800 \text{ nm} \pm 5 \text{ nm}$ ). SMF: single mode fiber with diameter of  $5 \mu\text{m}$ .

$\{p_i\}$ . Besides, we need six holograms to mimic the single-state part, namely  $|0\rangle\langle 0|$ , whose emerging probability is denoted as  $\{p_s\}$ . Finally, an extra hologram is added to represent the maximally entangled state, the probability of which is written as  $\{p_e\}$ .

Since the exposure time  $t$  of each hologram is fixed, to calculate the emerging probabilities of different holograms for given  $p$  and  $r$ , we need to consider a certain time interval  $T$ . During this time interval, the hologram corresponding to the maximally entangled state shall emerge  $pT/t$  times, while the product state shall emerge  $(1-p)[r+2(1-r)]T/t$  times, so that the relative probability between the maximally entangled state and the product state is  $p/\{(1-p)[r+2(1-r)]\}$ , which leads to  $p_e = p/[(1-p)(2-r)+p]$ . Consequently, the probability of the product part is given by  $p_p = 1 - p_e$ . Likewise, within the product state, the emerging ratio  $\eta$  between the single-state part and the isotropic part of the product state is  $\eta = r/2(1-r)$ , finally we obtain  $p_s = \eta p_p/6$  and  $p_i = (1-\eta)p_p/36$ .

In practice, the sampling procedure involves four random generators, which we denote as  $\lambda_{1,2,3,4}$ . If  $\lambda_1 \leq p_e$ , the hologram corresponding to the maximally entangled state will be selected and added as a frame to the animation. Otherwise if  $\lambda_1 > p_e$ , which indicates the product state, the second random generator  $\lambda_2$  is needed to de-

termine whether the single-state or the isotropic part is selected. In this case, if  $\lambda_2 \leq \eta$  and  $\lambda_3 \in \frac{1}{6}[\alpha-1, \alpha]$  where  $\alpha \in \{1, 2, \dots, 6\}$ , the  $\alpha_{\text{th}}$  hologram of the single-state part will be selected. However, if  $\lambda_2 > \eta$ , and  $\lambda_4 \in \frac{1}{36}[\beta-1, \beta]$  where  $\beta \in \{1, 2, \dots, 36\}$ , the  $\beta_{\text{th}}$  hologram of the isotropic part will be selected. After several rounds of sampling, we can eventually construct an animation corresponding to the specified axial state. It is worth stressing that although each frame in the animation is fixed, the random sampling ensures that it is impossible to predict which of these frames would be applied to the incident photon, thus the overall effect of the animation indeed mimics the stochastic process statistically.

*Results.*—With the above setup, we have selected ten targeted states with the configured parameters  $p_{\text{cfg}}$  and  $r_{\text{cfg}}$ , and the distribution are shown in the embedded inset in Fig. 3. Then, an over-complete quantum state tomography (see S3 of Supplemental Material for detailed results [37]) is employed to reconstruct the states and then evaluate the corresponding critical radii  $r_{AB}$  and  $r_{BA}$ .

The parameters of the actual reconstructed experimental states are shown in Fig. 3. One sees a significant deviation of the states 1, 6 and 10 from the configured parameters. This is due to the inherent fluctuation of the OAM modes generated by the BBO crystal and the environ-

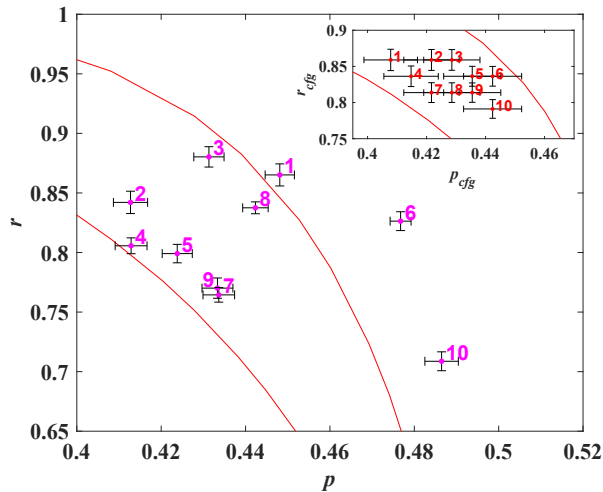


FIG. 3. Distribution of experimentally reconstructed states. Parameters  $p$  and  $r$  are retrieved from the reconstructed density matrices, which are denoted by the magenta dots. For comparison, the inset presents the parameter configuration  $p_{\text{cfg}}$  and  $r_{\text{cfg}}$  of the ten targeted states, which are denoted by the red dots. The uncertainties of  $p$  and  $r$  are obtained from the bootstrapping simulation with 20 variations on each of the experimental over-complete tomography results. The uncertainties of  $p_{\text{cfg}}$  and  $r_{\text{cfg}}$  are induced by the inherent nonequilibrium of photon numbers between the maximally entangled state and the product state, see S4 in Supplemental Material [37] for details. The deviation between the obtained states and the targeted states is also affected by the shot noise and crosstalk of the OAM measurement bases.

mental disturbance, which make the states even deviating into the two-way steerable area (see details in S4 of Supplemental Material [37]). In fact, these deviated states can be taken as a reference in eliminating the ambiguities comparing to existing data. It is important to emphasize again that with inappropriate assumptions, even when the reconstructed parameters are in the one-way steerable region, it is unclear that the corresponding states are one-way steerable and vice versa. (see discussion on the ambiguity in S1 of Supplemental Material [37]). Yet in our experiment, we show that this ambiguity is clarified as illustrated in Fig. 4, where one observes that all the critical radius of the ten states, where the red dots and blue squares refer to the steering direction from  $A$  to  $B$ , and from  $B$  to  $A$ , respectively. The deviated states 6 and 10 which lie in the two-way steerable area are indeed two-way steerable, while state 1 crosses the boundary of steering from  $B$  to  $A$  as it lies outside but close to the one-way steerable area. On the contrary, all other states which lie in exactly the one-way steerable area faithfully demonstrate the steering from  $A$  to  $B$  is possible, but the reverse is not. To sum up, our experiment successfully demonstrates one-way EPR-steering with a unified criterion. Comparing to the existing works, our work with

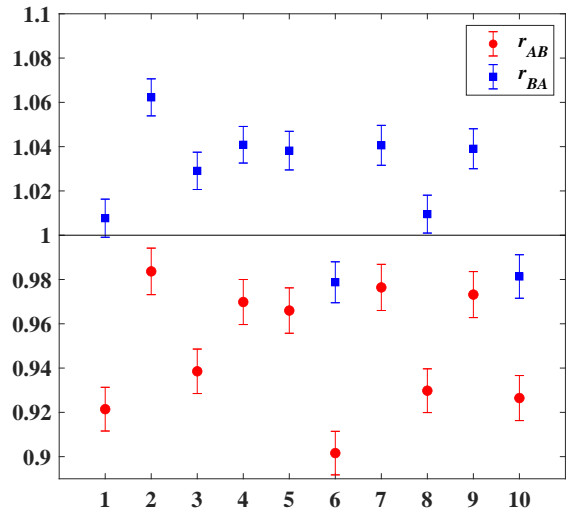


FIG. 4. Experimental results of one-way EPR steering certification. Number 1 to 10 denote the ten obtained states. Red dots refer to the case of Alice steering Bob, and blue squares refer to the opposite direction. As we mentioned, one can conclude steerability in certain direction if and only if the corresponding critical radius is less than 1. Clearly, the critical radii of the states except 1, 6 and 10 in two opposite directions distinctly lie in the separate zones, which reliably demonstrate the one-way steering effect. For state 1, its  $r_{AB}$  shows some ambiguity as the error bar crosses the boundary. For state 6 and 10, both  $r_{AB}$  and  $r_{BA}$  are less than 1, which indicates two-way steerable.

general POVM not only eliminate the restriction of the number of measurement settings [35, 36], but also remove the subtlety in the ancillary dimensionality in claiming one-way steerability.

*Conclusion.*—We have reported a reliable experimental demonstration of one-way quantum steering in the symmetric two-qubit entangled system based on an OAM platform. This resolves the ambiguity in the existing data demonstrating the directional nature of quantum steering in the lowest dimension.

Moreover, we emphasize that the precise parameter manipulation of the 1WS states does not only benefit the understanding of the nature of one-way steering, but also is applicable in particular quantum information processing tasks, such as the one-sided device-independent quantum key distribution [26].

We are grateful to Howard Wiseman, Chuan-Feng Li, and Ya Xiao for helpful discussions. We especially thank the authors of Ref. [36] for providing us with their experiment data and useful discussions. This work was supported by the National Key R&D Program of China under Grant No. 2017YFA0303800 and the National Natural Science Foundation of China through Grant Nos. 11574031, 61421001, and 11805010. Q.Z. acknowl-

edges support by the Office of China Postdoctoral Council The International Postdoctoral Exchange Fellowship Program (Grant No. 20190096). J.S. also acknowledges support by the Beijing Institute of Technology Research Fund Program for Young Scholars. H.C.N. is supported by the Deutsche Forschungsgemeinschaft (DFG, German Research Foundation - 447948357) and the ERC (Consolidator Grant 683107/TempoQ).

\* [jiangwei.shang@bit.edu.cn](mailto:jiangwei.shang@bit.edu.cn)

† [chau.nguyen@uni-siegen.de](mailto:chau.nguyen@uni-siegen.de)

‡ [zhangxd@bit.edu.cn](mailto:zhangxd@bit.edu.cn)

- [1] A. Einstein, B. Podolsky, and N. Rosen, Can quantum-mechanical description of physical reality be considered complete?, *Phys. Rev.* **47**, 777 (1935).
- [2] H. M. Wiseman, S. J. Jones, and A. C. Doherty, Steering, entanglement, nonlocality, and the Einstein-Podolsky-Rosen paradox, *Phys. Rev. Lett.* **98**, 140402 (2007).
- [3] S. Jones, H. Wiseman, and A. Doherty, Entanglement, Einstein-Podolsky-Rosen correlations, Bell nonlocality, and steering, *Phys. Rev. A* **76**, 052116 (2007).
- [4] D. J. Saunders, S. J. Jones, H. M. Wiseman, and G. J. Pryde, Experimental EPR-steering using Bell-local states, *Nat. Phys.* **6**, 845 (2010).
- [5] M. D. Reid, P. D. Drummond, E. G. Cavalcanti, P. K. Lam, H. A. Bachor, U. L. Andersen, and G. Leuchs, Colloquium: The Einstein-Podolsky-Rosen paradox: From concepts to applications, *Rev. Mod. Phys.* **81**, 1727 (2009).
- [6] S. P. Walborn, A. Salles, R. M. Gomes, F. Toscano, and P. H. Souto Ribeiro, Revealing Hidden Einstein-Podolsky-Rosen Nonlocality, *Phys. Rev. Lett.* **106**, 130402 (2011).
- [7] Q. Y. He, P. D. Drummond, and M. D. Reid, Entanglement, EPR steering, and Bell-nonlocality criteria for multipartite higher-spin systems, *Phys. Rev. A* **83**, 032120 (2011).
- [8] B. Wittmann, S. Ramelow, F. Steinlechner, N. K. Langford, N. Brunner, H. M. Wiseman, R. Ursin, and A. Zeilinger, Loophole-free Einstein-Podolsky-Rosen experiment via quantum steering, *New J. Phys.* **14**, 053030 (2012).
- [9] J.-L. Chen, X.-J. Ye, C. Wu, H.-Y. Su, A. Cabello, L. C. Kwak, and C. H. Oh, All-versus-nothing proof of Einstein-Podolsky-Rosen steering, *Scientific reports* **3**, 02143 (2013).
- [10] Q. Y. He and M. D. Reid, Genuine Multipartite Einstein-Podolsky-Rosen Steering, *Phys. Rev. Lett.* **111**, 250403 (2013).
- [11] P. Skrzypczyk, M. Navascués, and D. Cavalcanti, Quantifying Einstein-Podolsky-Rosen Steering, *Phys. Rev. Lett.* **112**, 180404 (2014).
- [12] H. Zhu, M. Hayashi, and L. Chen, Universal Steering Criteria, *Phys. Rev. Lett.* **116**, 070403 (2016).
- [13] H. C. Nguyen and T. Vu, Nonseparability and steerability of two-qubit states from the geometry of steering outcomes, *Phys. Rev. A* **94**, 012114 (2016).
- [14] S. Armstrong, M. Wang, R. Y. Teh, Q. Gong, Q. He, J. Janousek, H.-A. Bachor, M. D. Reid, and P. K. Lam, Multipartite Einstein-Podolsky-Rosen steering and genuine tripartite entanglement with optical networks, *Nat. Phys.* **11**, 167 (2015).
- [15] T. J. Baker, S. Wollmann, G. J. Pryde, and H. M. Wiseman, Necessary condition for steerability of arbitrary two-qubit states with loss, *Journal of Optics* **20**, 034008 (2018).
- [16] R. Uola, A. C. S. Costa, H. C. Nguyen, and O. Gühne, Quantum steering, *Rev. Mod. Phys.* **92**, 015001 (2020).
- [17] R. Horodecki, P. Horodecki, M. Horodecki, and K. Horodecki, Quantum entanglement, *Reviews of Modern Physics* **81**, 865 (2009).
- [18] V. Vedral, M. B. Plenio, M. A. Rippin, and P. L. Knight, Quantifying entanglement, *Phys. Rev. Lett.* **78**, 2275 (1997).
- [19] N. Brunner, D. Cavalcanti, S. Pironio, V. Scarani, and S. Wehner, Bell nonlocality, *Reviews of Modern Physics* **86**, 419 (2014).
- [20] D. Collins, N. Gisin, N. Linden, S. Massar, and S. Popescu, Bell Inequalities for Arbitrarily High-Dimensional Systems, *Phys. Rev. Lett.* **88**, 040404 (2002).
- [21] A. C. Dada, J. Leach, G. S. Buller, M. J. Padgett, and E. Andersson, Experimental high-dimensional two-photon entanglement and violations of generalized Bell inequalities, *Nat. Phys.* **7**, 677 (2011).
- [22] S. L. W. Midgley, A. J. Ferris, and M. K. Olsen, Asymmetric Gaussian steering: When Alice and Bob disagree, *Phys. Rev. A* **81**, 022101 (2010).
- [23] E. G. Cavalcanti, M. J. W. Hall, and H. M. Wiseman, Entanglement verification and steering when Alice and Bob cannot be trusted, *Phys. Rev. A* **87**, 032306 (2013).
- [24] J. Bowles, T. Vértesi, M. T. Quintino, and N. Brunner, One-way Einstein-Podolsky-Rosen Steering, *Phys. Rev. Lett.* **112**, 200402 (2014).
- [25] J. Bowles, F. Hirsch, M. T. Quintino, and N. Brunner, Sufficient criterion for guaranteeing that a two-qubit state is unsteerable, *Phys. Rev. A* **93**, 022121 (2016).
- [26] C. Branciard, E. G. Cavalcanti, S. P. Walborn, V. Scarani, and H. M. Wiseman, One-sided device-independent quantum key distribution: Security, feasibility, and the connection with steering, *Phys. Rev. A* **85**, 010301 (2012).
- [27] D. Cavalcanti, P. Skrzypczyk, G. H. Aguilar, R. V. Nery, P. H. S. Ribeiro, and S. P. Walborn, Detection of entanglement in asymmetric quantum networks and multipartite quantum steering, *Nat Commun* **6**, 7941 (2015).
- [28] T. J. Baker and H. M. Wiseman, Necessary conditions for steerability of two qubits from consideration of local operations, *Phys. Rev. A* **101**, 022326 (2020).
- [29] S. Jevtic, M. J. W. Hall, M. R. Anderson, M. Zwiernik, and H. M. Wiseman, Einstein-Podolsky-Rosen steering and the steering ellipsoid, *Journal of the Optical Society of America B* **32**, A40 (2015).
- [30] H. C. Nguyen, H.-V. Nguyen, and O. Gühne, Geometry of Einstein-Podolsky-Rosen correlations, *Phys. Rev. Lett.* **122**, 240401 (2019).
- [31] V. Händchen, T. Eberle, S. Steinlechner, A. Sambrowski, T. Franz, R. F. Werner, and R. Schnabel, Observation of one-way Einstein-Podolsky-Rosen steering, *Nat. Photon.* **6**, 596 (2012).
- [32] C.-M. Li, K. Chen, Y.-N. Chen, Q. Zhang, Y.-A. Chen, and J.-W. Pan, Genuine high-order Einstein-Podolsky-Rosen steering, *Phys. Rev. Lett.* **115**, 010402 (2015).

- [33] S. Wollmann, N. Walk, A. J. Bennet, H. M. Wiseman, and G. J. Pryde, Observation of genuine one-way Einstein-Podolsky-Rosen steering, *Phys. Rev. Lett.* **116**, 160403 (2016).
- [34] N. Tischler, F. Ghafari, T. J. Baker, S. Slussarenko, R. B. Patel, M. M. Weston, S. Wollmann, L. K. Shalm, V. B. Verma, S. W. Nam, H. C. Nguyen, H. M. Wiseman, and G. J. Pryde, Conclusive experimental demonstration of one-way Einstein-Podolsky-Rosen steering, *Phys. Rev. Lett.* **121**, 100401 (2018).
- [35] K. Sun, X.-J. Ye, J.-S. Xu, X.-Y. Xu, J.-S. Tang, Y.-C. Wu, J.-L. Chen, C.-F. Li, and G.-C. Guo, Experimental quantification of asymmetric Einstein-Podolsky-Rosen steering, *Phys. Rev. Lett.* **116**, 160404 (2016).
- [36] Y. Xiao, X.-J. Ye, K. Sun, J.-S. Xu, C.-F. Li, and G.-C. Guo, Demonstration of multisetting one-way Einstein-Podolsky-Rosen steering in two-qubit systems, *Phys. Rev. Lett.* **118**, 140404 (2017).
- [37] See supplemental material at \*\*\* for the detailed discussions on ambiguity of existing data, schematic of real scale experimental platform, parameter configuration and deviation and over-complete tomography results.
- [38] L. Allen, M. W. Beijersbergen, R. J. C. Spreeuw, and J. P. Woerdman, Orbital angular momentum of light and the transformation of Laguerre-Gaussian laser modes, *Phys. Rev. A* **45**, 8185 (1992).
- [39] E. Karimi, B. Piccirillo, E. Nagali, L. Marrucci, and E. Santamato, Efficient generation and sorting of orbital angular momentum eigenmodes of light by thermally tuned q-plates, *Applied Physics Letters* **94**, 231124 (2009).
- [40] E. Nagali, F. Sciarrino, F. De Martini, L. Marrucci, B. Piccirillo, E. Karimi, and E. Santamato, Quantum Information Transfer from Spin to Orbital Angular Momentum of Photons, *Phys. Rev. Lett.* **103**, 013601 (2009).
- [41] E. Karimi, J. Leach, S. Slussarenko, B. Piccirillo, L. Marrucci, L. Chen, W. She, S. Franke-Arnold, M. J. Padgett, and E. Santamato, Spin-orbit hybrid entanglement of photons and quantum contextuality, *Physical Review A* **82**, 022115 (2010).
- [42] Y. S. Rumala, G. Milione, T. A. Nguyen, S. Pratavieira, Z. Hossain, D. Nolan, S. Slussarenko, E. Karimi, L. Marrucci, and R. R. Alfano, Tunable supercontinuum light vector vortex beam generator using a q-plate, *Opt. Lett.* **38**, 5083 (2013).
- [43] S. Slussarenko, E. Karimi, B. Piccirillo, L. Marrucci, and E. Santamato, Efficient generation and control of different-order orbital angular momentum states for communication links, *J. Opt. Soc. Am. A* **28**, 61 (2011).
- [44] Q. Zeng, T. Li, X. Song, and X. Zhang, Realization of optimized quantum controlled-logic gate based on the orbital angular momentum of light, *Optics Express* **24**, 8186 (2016).
- [45] M. Agnew, J. Leach, M. McLaren, F. S. Roux, and R. W. Boyd, Tomography of the quantum state of photons entangled in high dimensions, *Phys. Rev. A* **84**, 062101 (2011).
- [46] Q. Zeng, B. Wang, P. Li, and X. Zhang, Experimental high-dimensional Einstein-Podolsky-Rosen steering, *Phys. Rev. Lett.* **120**, 030401 (2018).

## S1 Ambiguity in the one-way steering data for two-qubit systems

As we mentioned in the maintext, except for the recent experiment reported in Ref. [34], one-way steering experiments for qubit-qubit system are proved to inconclusive. This issue in fact has been discussed in Ref. [34], which demonstrates one-way steering of a qubit-qutrit system. Within qubit-qubit systems, the experiments remain inconclusive. This remains true even when only ideal measurements are considered.

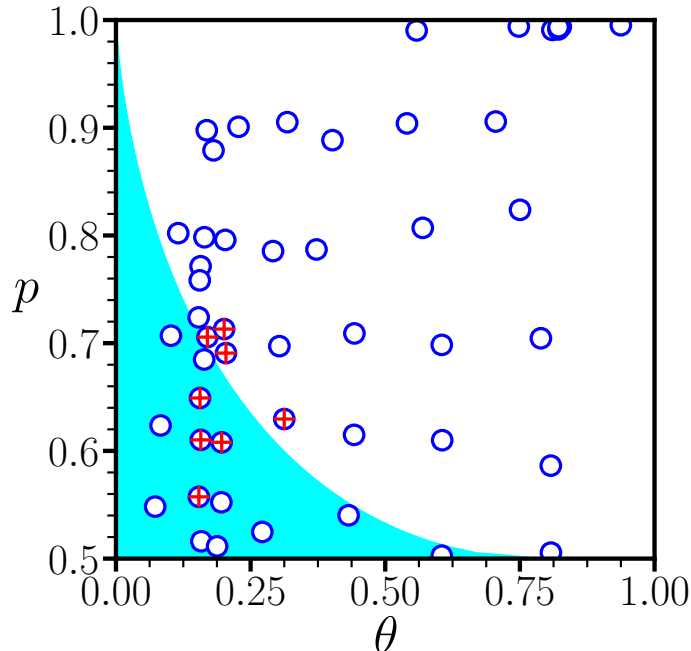


FIG. 5. Reconstructed parameters of states reconstructed from data from Ref. [36]. Out of 14 states (blue circles) which have the estimated parameters in the one-way steering area (cyan), there are only 4 states that are proven to be unsteerable (red cross). Note that the indicated one-way steering area is only a inner bound of the true one-way steering area, thus there are also states outside this areas which turn out to be one-way steerable.

To illustrate the issue, we take the experiment reported in Ref. [36]. Although this experiment concentrates on one-way steering with finite number of measurements imposed on Alice's side, it also contains the data for all ideal measurements. The state under consideration is

$$\rho = p|\theta\rangle\langle\theta| + (1-p)\mathbb{I}_A \otimes \rho_B, \quad (5)$$

where  $|\theta\rangle = \cos\theta|00\rangle + \sin\theta|11\rangle$  and  $\rho_B = \text{Tr}_A[|\theta\rangle\langle\theta|]$ . It has been shown in Ref. [25] that for  $p > 1/2$  and  $\cos^2(2\theta) \geq (2p-1)/[(2-p)p^3]$ , the state is steerable from  $A$  to  $B$ , but unsteerable from  $B$  to  $A$ . With the experimental data obtained in Ref. [36], we can reconstruct 50 states. The corresponding parameters  $\theta$  and  $p$  are inferred to a high accuracy. Out of 50 states, 14 have the reconstructed parameters falling into the one-way steerable area. However, the claim that these states are one-way steerable is in fact incorrect. This is because the reconstructed parameters of the states are only two out of 15 independent parameters of a general two-qubit states. Experimental deviations present not only in the two parameters  $\theta$  and  $p$ , but in all other possible parameters. The deviation in the other parameters may make the states two-way steerable or two-way unsteerable despite the fact the the two parameters  $\theta$  and  $p$  fall within the one-way steerable area.

To examine this, we consider the tomography of the experimental states based on the obtained data. The critical radii of the states are computed, showing that 10 of the states that has two indicated parameters in the one-way steerable area are in fact not one-way steerable (see Fig 5).

## S2 Real scale experimental platform

In Fig. 6, we show the real scale schematic of our experimental platform.

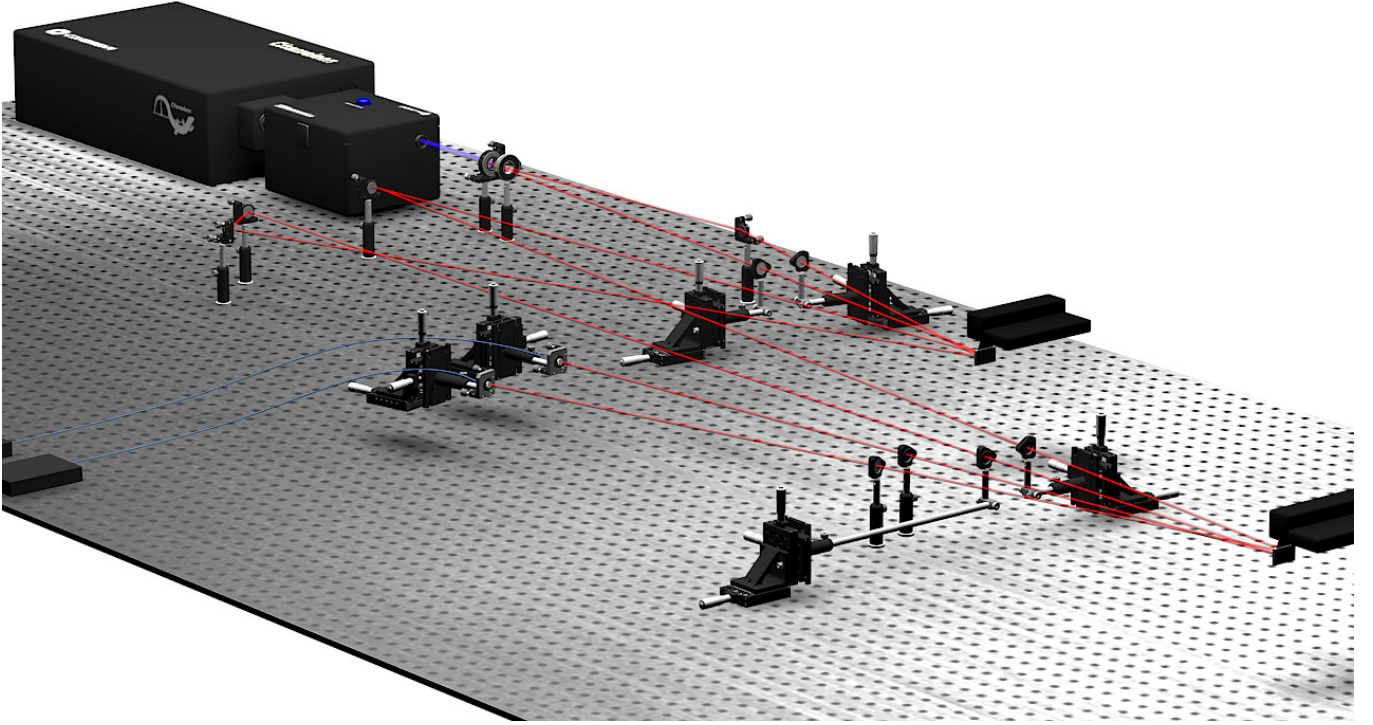


FIG. 6. Real scale experimental platform. The supports of spatial light modulators are omitted for better viewing.

### S3 Over-complete quantum state tomography

In this section, we show the tomography results of the ten targeted states by using an over-complete quantum state tomography scheme. Figure 7 shows the reconstructed density matrices. It is worthy noting that fidelity can work as reference yet drawing conclusions based on high fidelities can be problematic [34].



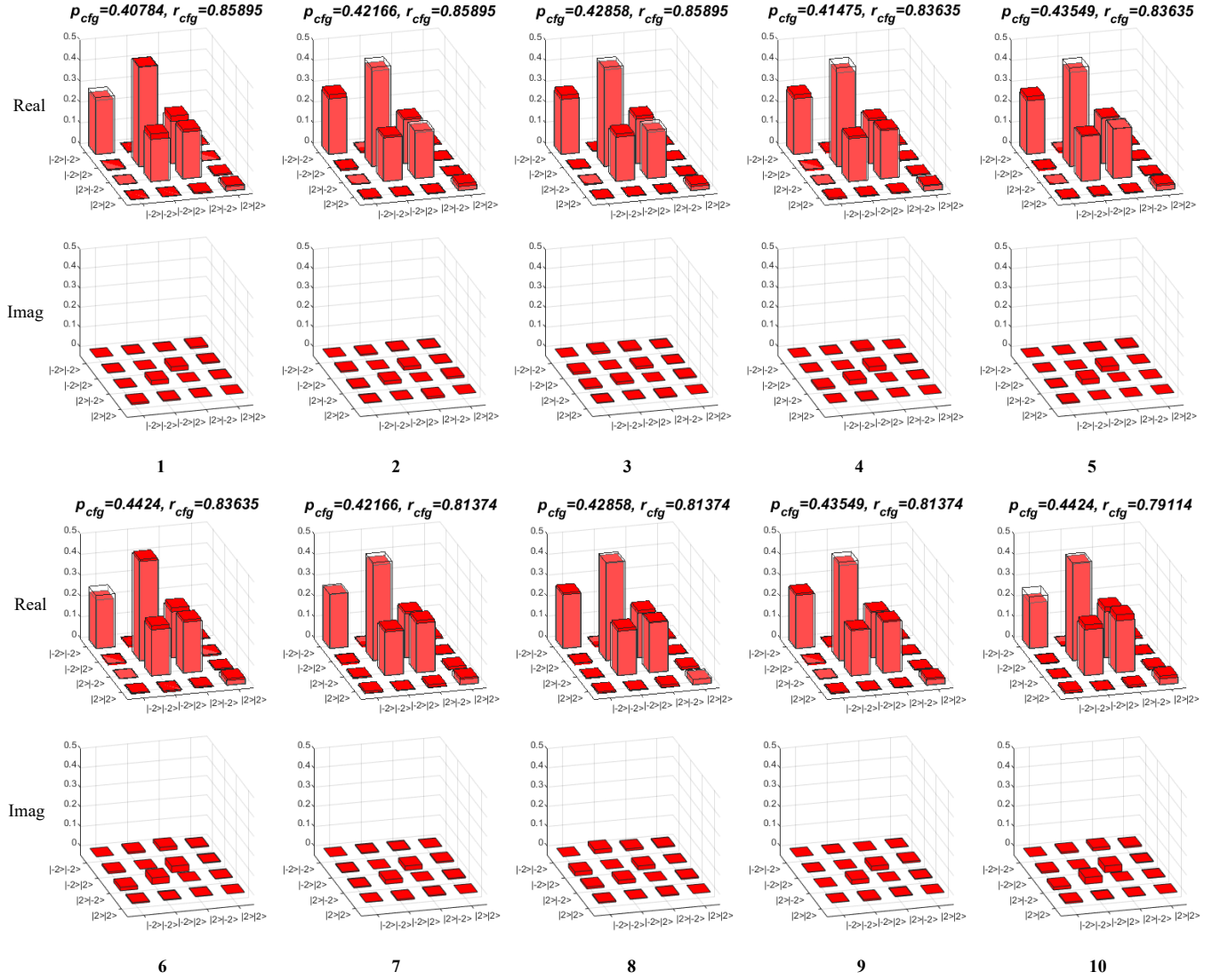


FIG. 7. Reconstructed density matrices of the ten targeted states. The solid red bars refer to reconstructed states' density matrices, and the transparent wireframe bars refer to configured targeted states' density matrices.

#### S4 Parameter configuration and deviation between the reconstructed states and the targeted states

In our animation construction, we prepare the involved computer-generated holograms (CGH) in advance and form the random pool. We then select one of those CGHs to append as the frame of the animation according to the sampling rules described in the maintext. In the parameter configurations, the number of photons corresponding to the maximally entangled state and the number of photons which are transformed to simulate the product state are supposed to be equal. However, in practice, due to the inherent unbalanced distribution of the OAM modes under the SPDC process and the different collecting efficiency between these two types of photons, these two numbers are slightly different. Specifically, the ratio between these two numbers in our experiment is  $\alpha = 1.106 \pm 0.0246$ . Consequently, we have  $p_{\text{cfg}} = p_{\text{ipt}} * \alpha$  and  $r_{\text{cfg}} = r_{\text{ipt}} / \alpha$ , where  $p_{\text{cfg}}(r_{\text{cfg}})$  is the parameter we aim to achieve when we input  $p_{\text{ipt}}(r_{\text{ipt}})$ . In Table I, we list all the parameter settings in detail. The significant fluctuation of the ratio is thus the main cause of the deviation between the obtained and the targeted states. Note that the deviation is also affected by the shot noise and crosstalk of the OAM measurement bases.

TABLE I. Parameter settings of the ten targeted states.

	1	2	3	4	5
$p_{\text{ipt}}$	0.36875	0.38125	0.3875	0.375	0.39375
$r_{\text{ipt}}$	0.95	0.95	0.95	0.925	0.925
$p_{\text{cfg}}$	$0.4078 \pm 0.0091$	$0.4217 \pm 0.0094$	$0.4286 \pm 0.0095$	$0.4148 \pm 0.0092$	$0.4355 \pm 0.0097$
$r_{\text{cfg}}$	$0.859 \pm 0.0234$	$0.859 \pm 0.0234$	$0.859 \pm 0.0234$	$0.8363 \pm 0.0228$	$0.8363 \pm 0.0228$
Fidelity <sup>a</sup>	$0.9964 \pm 0.0008$	$0.9956 \pm 0.0006$	$0.9957 \pm 0.0007$	$0.9960 \pm 0.0006$	$0.9963 \pm 0.0004$
	6	7	8	9	10
$p_{\text{ipt}}$	0.4	0.38125	0.3875	0.39375	0.4
$r_{\text{ipt}}$	0.925	0.9	0.9	0.9	0.875
$p_{\text{cfg}}$	$0.4424 \pm 0.0098$	$0.4217 \pm 0.0094$	$0.4286 \pm 0.0095$	$0.4355 \pm 0.0097$	$0.4424 \pm 0.0098$
$r_{\text{cfg}}$	$0.8363 \pm 0.0228$	$0.8137 \pm 0.0221$	$0.8137 \pm 0.0221$	$0.8137 \pm 0.0221$	$0.7911 \pm 0.0215$
Fidelity	$0.9960 \pm 0.0005$	$0.9966 \pm 0.0006$	$0.9970 \pm 0.0005$	$0.9958 \pm 0.0013$	$0.9951 \pm 0.0005$

<sup>a</sup> The fidelity is defined as  $[\text{Tr}(\sqrt{\sqrt{\rho}\rho_0\sqrt{\rho}})]^2$ .